



HAL
open science

Parametric Design Approach for Wireless Power Transfer System: UAV Applications

Mohammed Terrah, Mostafa-Kamel Smail, Lionel Pichon, Mohamed Bensetti

► To cite this version:

Mohammed Terrah, Mostafa-Kamel Smail, Lionel Pichon, Mohamed Bensetti. Parametric Design Approach for Wireless Power Transfer System: UAV Applications. *Drones*, 2024, 8, pp.735. 10.3390/drones8120735 . hal-04823139

HAL Id: hal-04823139

<https://hal.science/hal-04823139v1>

Submitted on 6 Dec 2024

HAL is a multi-disciplinary open access archive for the deposit and dissemination of scientific research documents, whether they are published or not. The documents may come from teaching and research institutions in France or abroad, or from public or private research centers.





L'archive ouverte pluridisciplinaire **HAL**, est destinée au dépôt et à la diffusion de documents scientifiques de niveau recherche, publiés ou non, émanant des établissements d'enseignement et de recherche français ou étrangers, des laboratoires publics ou privés.



Distributed under a Creative Commons Attribution 4.0 International License

Article

Parametric Design Approach for Wireless Power Transfer System: UAV Applications

Mohammed Terrah ^{1,2,3} , Mostafa-Kamel Smail ^{1,2,3,*} , Lionel Pichon ^{1,2}  and Mohamed Bensetti ^{1,2} 

¹ Laboratoire de Génie Electrique et Electronique de Paris (GeePs), CNRS, CentraleSupélec, Université Paris-Saclay, 91192 Gif-sur-Yvette, France; mohammed.terrah@centralesupelec.fr (M.T.); lionel.pichon@centralesupelec.fr (L.P.); mohamed.bensetti@centralesupelec.fr (M.B.)

² Laboratoire de Génie Electrique et Electronique de Paris (GeePs), CNRS, Sorbonne Université, 75252 Paris, France

³ Institut Polytechnique des Sciences Avancées Paris-IPSA, 94200 Ivry-sur-Seine, France

* Correspondence: mostafa-kamel.smail@centralesupelec.fr

Abstract: Adopting Wireless Power Transfer (WPT) technology to an Unmanned Aerial Vehicle (UAV) involves adding extra components, which may impact the drone's overall weight and performance. This paper aims to enhance UAV performance by designing a lightweight WPT system through a parametric design approach. This method explores novel perspectives by identifying the most suitable combination of parameters in terms of efficiency, weight, and feasibility. Various parameters such as the compensation topology, number of turns of coils, and frequency were studied. The system was analyzed through a coupled simulation approach, where electromagnetic modeling of the coupler using the finite element method (FEM) was combined with electrical circuit simulations, providing a more accurate assessment of the overall system efficiency and behavior considering variations in the coupling factor due to misalignment. A prototype of the resulting configuration was designed and tested experimentally versus misalignment at reduced power using a specific test bench. The results show a 70% efficiency level with SP compensation that was improved to 80% with SS compensation.

Keywords: Wireless Power Transfer; Unmanned Aerial Vehicle; compensation topology; frequency; efficiency; FEM modeling; misalignment



Citation: Terrah, M.; Smail, M.-K.; Pichon, L.; Bensetti, M. Parametric Design Approach for Wireless Power Transfer System: UAV Applications. *Drones* **2024**, *8*, 735. <https://doi.org/10.3390/drones8120735>

Academic Editor: Abdessattar Abdelkefi

Received: 23 October 2024
Revised: 25 November 2024
Accepted: 27 November 2024
Published: 5 December 2024



Copyright: © 2024 by the authors. Licensee MDPI, Basel, Switzerland. This article is an open access article distributed under the terms and conditions of the Creative Commons Attribution (CC BY) license (<https://creativecommons.org/licenses/by/4.0/>).

1. Introduction

UAVs have rapidly emerged as multipurpose indispensable tools in our modern era, bringing significant innovations in a variety of fields [1–3]. One of the sectors where UAVs have found an appealing application is inspection [4]. Whether in infrastructure, energy, agriculture or environmental monitoring, UAVs offer an efficient solution for inspecting hard-to-reach or potentially dangerous areas. Equipped with cutting-edge technology, UAVs can carry out detailed inspections and provide real-time data, enabling potential problems to be identified quickly, reducing operational costs, and minimizing risks to personnel. However, the limited autonomy of their batteries [5,6] and their dependence on physical recharging, often at the starting point, restrict the use of UAVs. This considerably reduces the overall duration of their missions. To extend the UAV's mission duration and automate the charging process, a WPT system based on resonant inductive coupling can be integrated into the UAV.

In previous papers, several researchers studied WPT for UAVs using different approaches. In [4], the authors investigated a WPT system for UAVs intended for transmission lines patrol with 100 W power and 83% efficiency. The authors in [7] proposed the addition of a buck converter before the load (the battery) to increase the charging current and reduce power losses, increasing system efficiency by 9%. In [8], the authors designed a magnetic coupler aiming at a lightweight receiver and low leakage flux, using a vertically placed

hollow coil and a bipolar magnetic field design. In [9], a three-phase WPT system was proposed to reduce electromagnetic interference. Additionally, ref. [10] proposed a new magnetic coupler for UAVs to improve magnetic coupling. However, these studies did not extensively explore the impact of misalignment considering the emitter coil size.

Other studies have explored innovative designs but did not adequately address the weight of the system components. In [11], the authors presented an UAV WPT system capable of delivering up to 70 W with a receiver in the form of a landing gear designed using an aluminum tube. Similarly, in [12], the authors investigated Series–Series (SS) and Series–Parallel (SP) compensation topologies to enhance efficiency while minimizing the coils' weight with a configuration that required the addition of extra landing gear and holders to fix the receiving coil. In [13], origami-deployable coils were introduced to enable wireless power transfer for UAVs using a system responsible for folding and unfolding the receiving coil.

Other related papers treated the weight and misalignment issues; unfortunately, the system's efficiency was not sufficiently developed. In [14], the authors proposed a dual-coil WPT system designed to maintain charging efficiency above 50% and address misalignment during landing, but the system experienced over 30% losses, which were left untreated. The study in [15] presented an optimized phase-shift modulation strategy for bidirectional inductive power transfer to minimize coil losses in an SS WPT circuit, but the overall system efficiency was not fully explored.

Other studies addressed also WPT. In [16], the authors explored various coupler topologies to identify the most efficient one for dynamic WPT. In the same concept, the authors in [17] analyzed different coil structures for WPT systems designed for UAV applications. The authors in [18] investigated the efficiency of a magnetic resonant WPT system in the conducting medium to develop a method for the determination of the optimal frequency for system design. Similarly, in [19], the authors focused on improving the efficiency and performance of inductive power transfer coils through an optimization approach. Their findings indicated that coupling mainly depends on the area enclosed by the coils and that their exact shape has only a minor influence. In [20], the authors studied the impact of the working frequency on WPT systems. The results showed that higher frequency results in a smaller coupler for the same transmitted power.

To enhance the current approaches, new perspectives were explored in this paper by studying the overall challenges encountered in WPT for UAVs aiming for a best compromise between high efficiency level, extending the misalignment range, adding minimum weight, and choosing an appropriate frequency for the WPT system all while maintaining UAV performance and aerodynamics. In order to so and design an effective WPT system with a short downtime during recharging, a novel parametric approach was introduced, considering key factors such as compensation topology, coils turns, and resonance frequency.

The work is divided into two main sections: modeling and simulation and experimental validation. In the modeling phase, the Finit Element Method (FEM) is used to design an electromagnetic model to determine the electrical parameters of the magnetic coupler. The electrical model was then simulated using electrical circuits simulator software, adopting a circuit-based approach to analyze the entire power chain and assess the power efficiency of the WPT system. For the experimental validation, the electrical parameters of the magnetic coupler were first measured, which was then followed by a comprehensive validation of the entire system through a mechanical test bench, allowing a thorough misalignment study.

2. UAV Overview

The WPT system is designed to be fitted to a DJI F450 UAV model, which operates without additional landing gear (Figure 1). One advantage of this UAV configuration is the close proximity of the coils, which improves the efficiency of WPT. Furthermore, adding extra landing gear could introduce additional weight to the drone and potentially lead to aerodynamic issues if the WPT system is not integrated correctly [21].

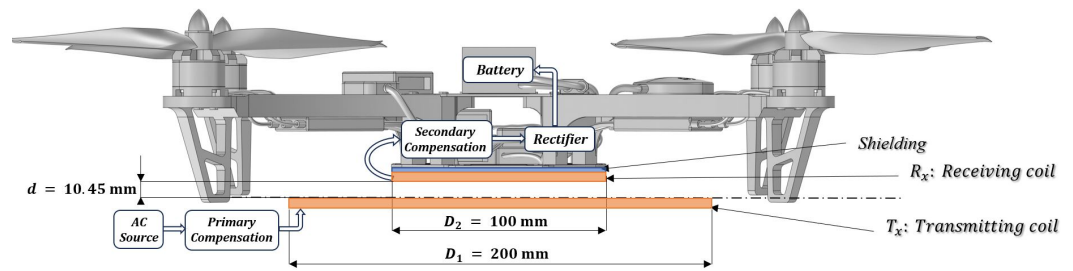


Figure 1. Representation of a WPT system for UAV.

3. WPT System Setup and Analysis

3.1. WPT System Configuration

The configuration of the WPT system is illustrated in Figure 1 and consists mainly of two parts: the transmitting part and the receiving part. In general, the primary part, contains an AC power supply and a transmitting coil T_x with a compensation capacitor C_1 . The secondary part consists of a battery, a rectifier for converting AC current to DC, and a receiving coil R_x with its compensation capacitor C_2 . A ferrite plate is placed right on top of the secondary coil to reinforce the coupling between the two coils and serve as a shielding for the on-board electronics.

One of the main challenges of WPT for UAVs is ensuring accurate landing, as this parameter depends directly on the precision of the UAV’s GPS. Inaccurate positioning can cause misalignment between the transmitting coil and the receiver, leading to weak power transfer. To mitigate this issue, the size of the transmitter coil was chosen to be twice that of the receiver coil, providing a larger effective area for WPT despite potential misalignment.

Coils were chosen to be circular planar since the distance between the two coils is small.

3.2. System’s Electrical Circuit

SP compensation topology was first adopted for the electrical circuit (Figure 2) due to its advantage of high coupler efficiency with a reduced number of turns at the receiving coil [12].

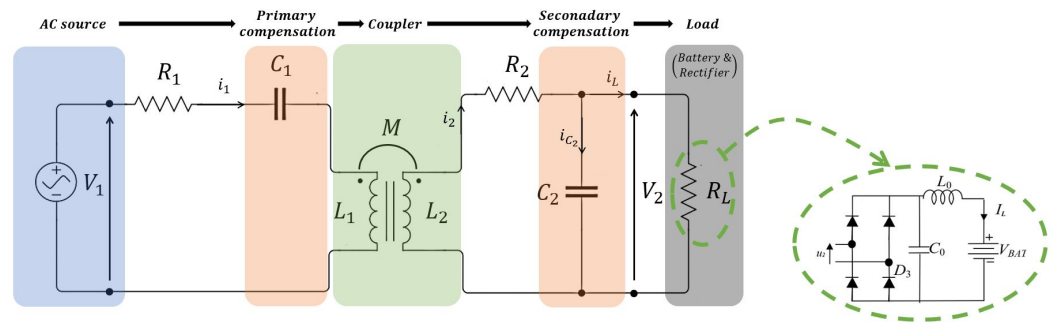


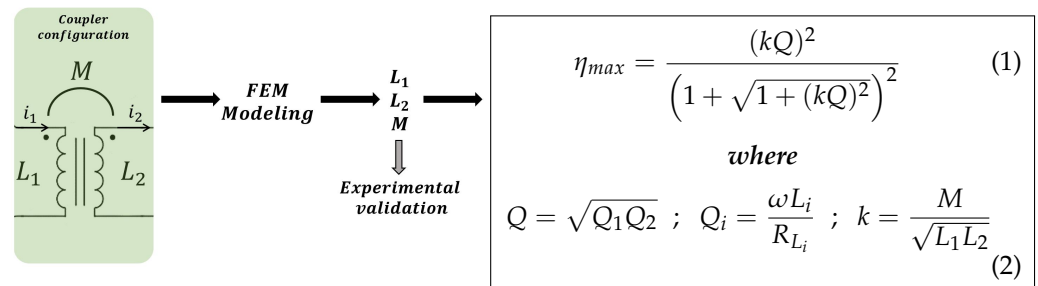
Figure 2. Electrical circuit of the WPT system.

Inspired by [12], the coupler configuration (Table 1) was adapted to the DJI F450 UAV model. This configuration was determined by electromagnetic modeling with an efficiency of over 80% estimated using Equation (1). For SP and SS compensation topology, Equation (1) represents the maximum efficiency that can be achieved by the coupler [19], where L_i and R_{L_i} are the respective self-inductances and resistances of the coils, M is the mutual inductance between coils, Q_i is the quality factor of the coils and k is the coupling factor between coils.

Table 1. UAV specifications.

UAV type	DJI F450
Distance between the UAV's bottom base and the floor	14.85 (mm)
Battery type	3S LiPo battery
Battery voltage V_{bat}	11.1 (V)
Battery capacity	5 (Ah)

Figure 3 illustrates the evaluation method used to identify an efficient coupler configuration. This approach allows for selecting the configuration with the required performance.

**Figure 3.** Coupler evaluation chart.

The characteristics of the coupler are described in Table 2. The radius of the Litz wire used to design the coils was chosen to withstand a current of 12 A that can allow up to a 2C charging rate of the UAV's battery.

Table 2. Coupler characteristics.

Parameter	Symbol	Value	Unit
Frequency	f	150	kHz
T_x external radius	r_{T_x}	100	mm
R_x external radius	r_{R_x}	50	mm
Distance between coils	d	10.45	mm
Ferrite plate thickness	e_f	2	mm
T_x number of turns	N_1	8	turns
R_x number of turns	N_2	2	turns
Litz wire characteristics		Strand diameter: 0.05 No. of strands: 1000	mm

Based on coupler characteristics, an FEM model of the coupler was developed to evaluate its efficiency and performance.

3.3. Electromagnetic Model of the Coupler

The aim of the electromagnetic model was to explore various coupler designs and configurations to maximize power transfer efficiency (Figure 4). This includes optimizing coil shapes and geometrical layouts. The 3D FEM model allows the analysis of the coupler performance by calculating the electrical parameters «self-inductances L_1, L_2 and mutual inductance M » versus misalignment from the design before producing physical prototypes.

The obtained values of L_1, L_2 and M are first used to estimate the maximum coupler efficiency « η_{max} » and then subsequently used in the electrical circuit to determine the power efficiency « η » of the WPT system both at resonance and out of resonance, as it is directly dependent on the misalignment.

Coils were simplified to homogenized multi-turn structures due to the complexity and CPU consumption involved in accurately modeling Litz wire [22].

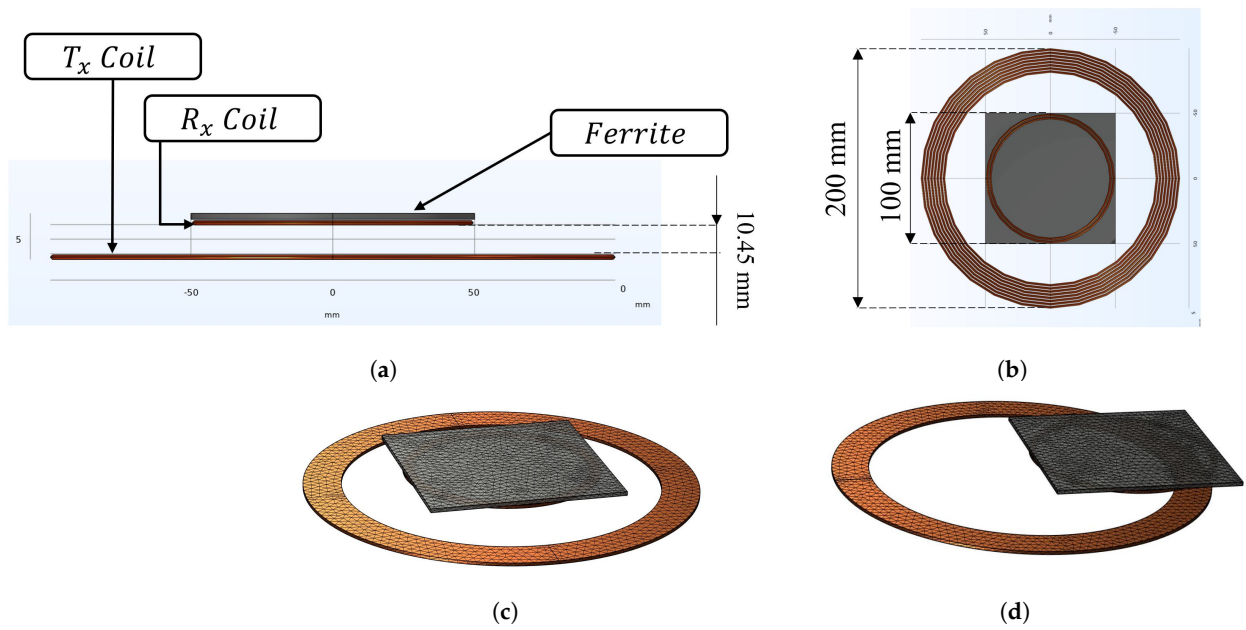


Figure 4. FEM geometry of the coupler: (a) Front view. (b) Bottom view. (c) 3D view of the coupler at $d_x = 0$ mm. (d) 3D view of the coupler at $d_x = 55$ mm.

3.4. Experimental Validation of the FEM Results

For experimental validation, the inductances L_1, L_2 and M were measured versus misalignment d_x via an RLC meter «Wayne Kerr 4300 series» (Figure 5c). The receiver coil was fixed to a mechanic arm to allow misalignment study.

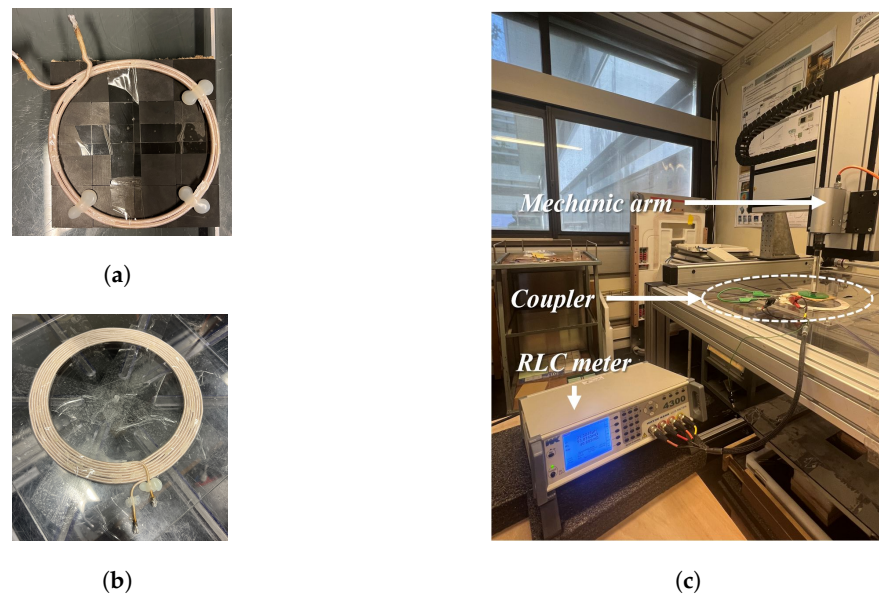


Figure 5. Experimental design and validation of the magnetic coupler prototype. (a) Receiving coil. (b) Transmitting coil. (c) RLC meter measurements.

Measurement methodology:

Based on the coupler’s electrical Equation (3), the concept is to make two series associations; the first with the windings in the same direction (Figure 6a), and the second with the windings in the opposite direction (Figure 6b). Winding resistances are neglected

in these measurements ($R_{L_1} = R_{L_2} = 0$). V_{L_1} , V_{L_2} and i_1 , i_2 represent the transmitter and receiver coil's voltages and currents, respectively.

$$\begin{cases} V_{L_1} = (R_{L_1} + j\omega L_1)i_1 + j\omega M \cdot i_2 \\ V_{L_2} = (R_{L_2} + j\omega L_2)i_2 + j\omega M \cdot i_1 \end{cases} \quad (3)$$

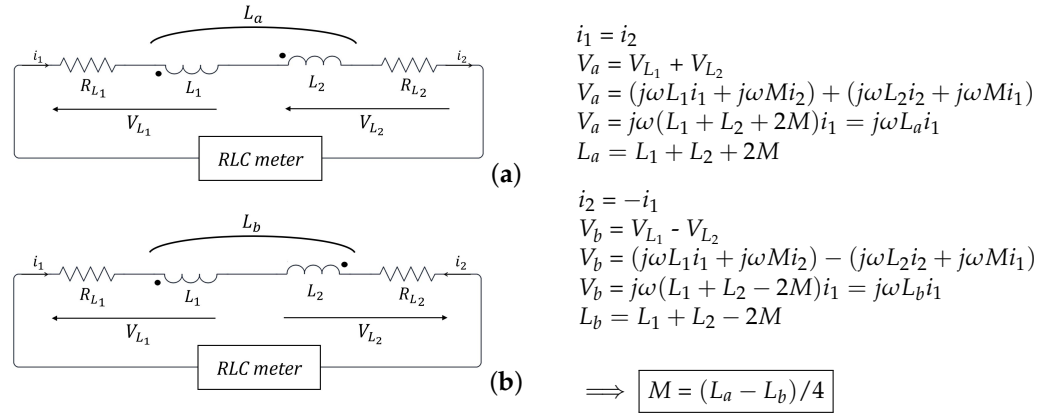


Figure 6. Coupler parameters measurement. (a) Series association in the same direction. (b) Series association in the opposite direction.

The measurements are then compared with the results from the FEM model. Figure 7 illustrates the variation of the system's main inductances versus misalignment. The FEM and experimental results show almost identical trends with less than 10% error. The primary self-inductance L_1 remains relatively constant despite misalignment with a slight increase beyond 50 mm due to the displacement of the ferrite above the receiver coil. Since the two coils are positioned closely together (10 mm apart), the ferrite above the receiving coil has an influence on the primary inductance.

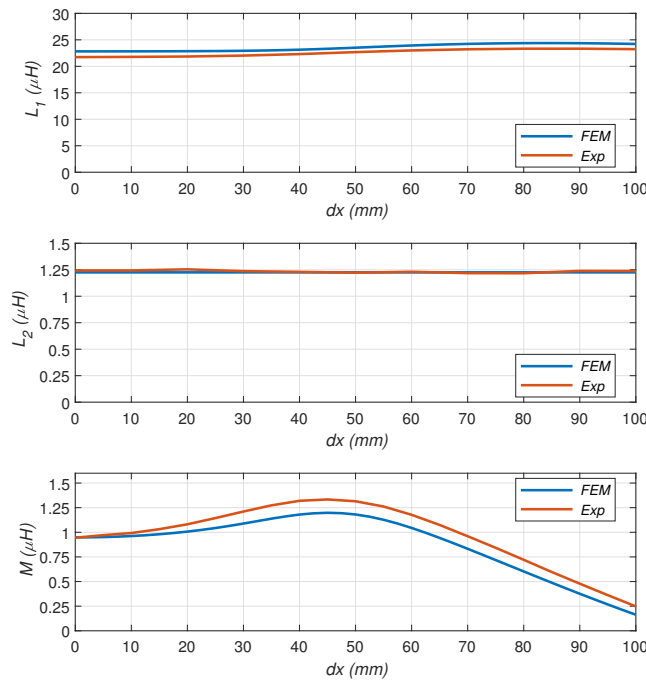


Figure 7. Coupler's inductances versus misalignment.

The secondary self-inductance L_2 remains unchanged versus misalignment, since it is fixed to the ferrite. With the receiver coil fixed below the ferrite, the ferrite maintains a constant impact on the L_2 versus misalignment.

For the mutual inductance M , a progressive increase is observed up to 50 mm misalignment, which is followed by a decrease beyond this point. This curve indicates that maximum coupling between the two coils occurs when their axes are misaligned by approximately 50 mm. This can be explained by the size difference between the coils. The receiver coil, being half the size of the transmitter coil, is able to capture a higher magnetic field density from the transmitter when misaligned compared to when the two coils are perfectly aligned.

3.5. Coupler Efficiency η_{max} Analysis

The maximum efficiency that the coupler can achieve Equation (1) was first estimated with FEM results using the FEM inductances and DC resistance of coils; however, at 150 kHz, the AC resistance of coils become significant, which is why the measured AC resistance of the coils and measured inductances were used for a real coupler efficiency estimation (Table 3).

Table 3. Coupler measured parameters.

Parameter	Symbol	Value	Unit
T_x self inductance at $d_x = 0$ mm	L_1	22.3	μH
R_x self inductance at $d_x = 0$ mm	L_2	1.27	μH
Mutual inductance at $d_x = 0$ mm	M	0.96	μH
T_x resistance	R_{L_1}	DC: 48.4 AC: 249	$\text{m}\Omega$
R_x resistance	R_{L_2}	DC: 7.5 AC: 18	$\text{m}\Omega$

Figure 8 illustrates the coupler's maximum efficiency as a function of misalignment. The curve shows an 80% efficiency from 0 mm to 70 mm of misalignment, reflecting strong coupling between the two coils. Beyond 70 mm, a drop in efficiency is observed up to 100 mm of misalignment explained by the weak coupling between coils seen in the mutual inductance curve (Figure 7).

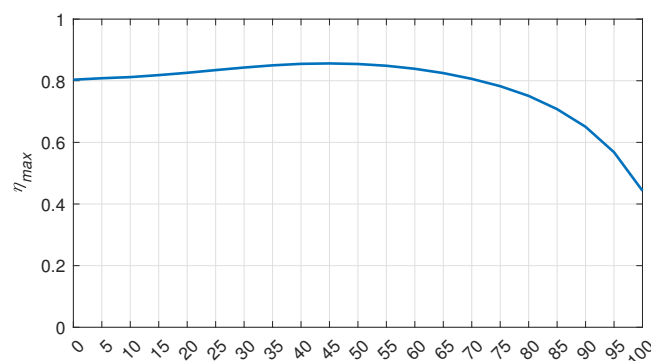


Figure 8. Maximum coupler efficiency versus misalignment.

The efficiency curve highlights the coupler's effective performance across varying levels of misalignment, leading to a further study of the overall energy efficiency of the WPT system under misalignment conditions.

3.6. WPT System Evaluation

In this section, an evaluation of the whole WPT system efficiency was developed. A simulation of the electrical circuit (Figure 2) on LTspice was carried out, and the efficiency of the system was calculated using Equation (4), which represents the ratio between the active power consumed by the load and the active power supplied by the charging station.

$$\eta = \frac{R_L \cdot i_{L_{rms}}^2}{V_{1_{rms}} \cdot i_{1_{rms}} \cdot \cos(\phi)} \quad (4)$$

A power « P_L » of 63 W was imposed at the load level R_L to charge the 3S battery (Figure 9) in 1 h, and a voltage of 12.6 V was set as the charging voltage « V_{bat} ». Based on these two parameters, the load equivalent resistance « R_L », which corresponds to the UAV's battery plus the AC/DC full bridge rectifier, was calculated at the first harmonic using Equation (5).



Figure 9. Battery of the UAV.

$$R_L = \frac{8 \cdot V_{bat}^2}{\pi^2 \cdot P_L} \quad (5)$$

As for compensation capacitors, according to [23,24], capacitors C_1 and C_2 are obtained via Equation (6) for SP compensation topology to ensure working at resonance.

$$C_1 = \frac{1}{\omega^2(L_1 - \frac{M^2}{L_2})} \quad \& \quad C_2 = \frac{1}{\omega^2 L_2} \quad (6)$$

The source power P_1 was adapted to ensure the 63 W load power with a limit of 120 W (Table 4). This AC power source is provided by a DC source followed by a half-bridge inverter, as shown in Figure 10. The inverter and its LTspice model were developed and provided in the laboratory.

Table 4. System characteristics.

Parameter	Symbol	Value	Unit
Source power	P_1	up to 120	W
Load power	P_L	up to 63	W
Battery charging voltage	V_{bat}	12.6	V
Load equivalent resistance	R_L	2.04	Ω
T_x self inductance at $d_x = 0$ mm	L_1	22.3	μH
R_x self inductance at $d_x = 0$ mm	L_2	1.27	μH
Mutual inductance at $d_x = 0$ mm	M	0.96	μH
Primary bloc resistance ($R_{L_1} + R_{C_1}$)	R_1	260	m Ω
Secondary bloc resistance ($R_{L_2} + R_{C_2}$)	R_2	53	m Ω
Primary compensation capacitor	C_1	53.27	nF
Secondary compensation capacitor	C_2	905	nF

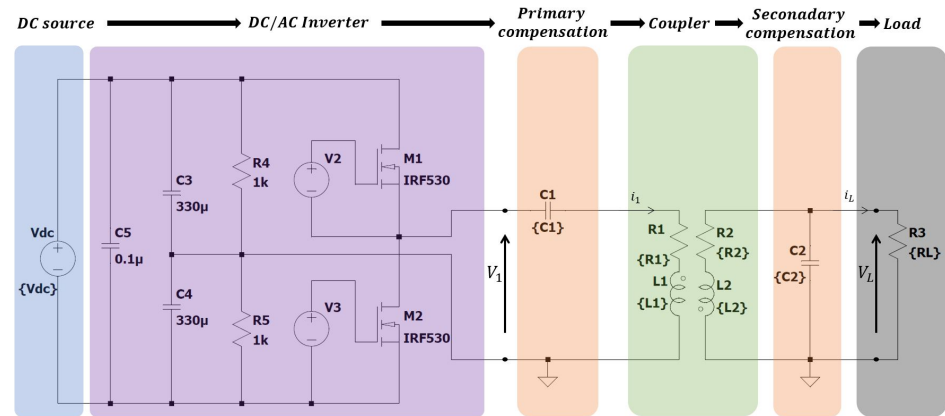


Figure 10. LTSpice model of the electrical circuit: SP compensation.

Real components values were measured and taken into consideration for a realistic simulation approach. Resistors R_1 and R_2 represent the total resistance of the primary and secondary blocks (series resistances of coils plus capacitors). The capacitors' equivalent series inductances (ESLs) were neglected compared to the coils' inductances.

The overall characteristics of the WPT system are summarized in Table 4.

Simulations versus misalignment were run. Figure 11 shows the source and load voltages and currents in the time domain. Both primary and load currents i_1 , i_L are in phase with their respective voltages V_1 and V_L ; this indicates an adequate compensation of inductive reactances and operation in resonance.

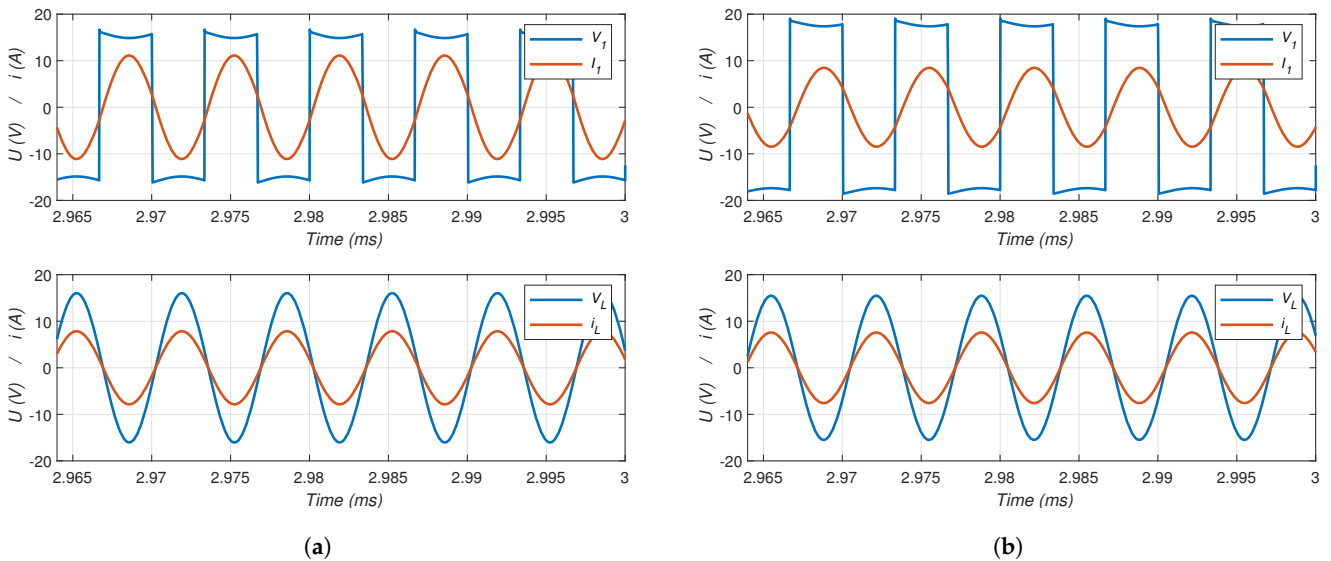


Figure 11. Source and load current and voltage of the simulation model. (a) At perfect alignment $d_x = 0$ mm. (b) At 65 mm misalignment.

At 65 mm misalignment (Figure 11b), a phase shift between the primary current and voltage begins to appear as the coils are further misaligned. This is due to weak coupling and variation in the mutual inductance M as a result of the secondary coil being further misaligned with the primary coil, which led to losing the compensation on the primary bloc.

Further simulations were ran, and power efficiency was calculated versus misalignment via RMS values of signals for each misalignment case to evaluate the system's response at misalignment conditions.

The efficiency curve (Figure 12) shows the same shape as the mutual inductance with an efficiency drop from 70 mm misalignment corresponding to weak coupling between coils. The efficiency level is approximately between 60 and 76% in the 0 to 70 mm misalignment

range; this is due to Joule losses in coils and in capacitors. One other reason for the efficiency drop from 70 mm misalignment is the phase shift between the source current and voltage (Figure 11b). This phase shift is the result of an incomplete compensation of reactive energy at the primary level. The incomplete compensation is caused by the relation between the primary compensation capacitor C_1 and the mutual inductance M (Equation (6)), which changes as a function of the misalignment. These results lead to pursuing the study with a different compensation topology that isolates the value of the capacitors from the mutual inductance with the aim of obtaining a WPT system that is more tolerant to misalignment and more effective for the UAV.

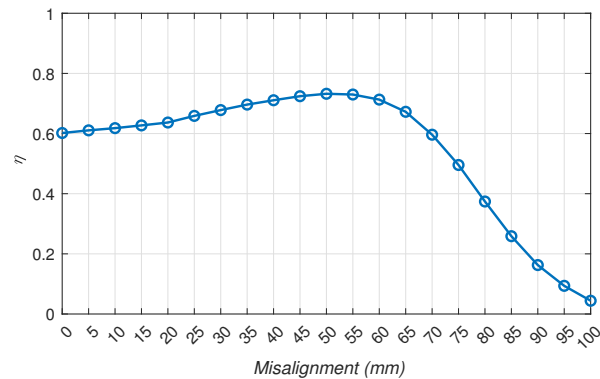


Figure 12. WPT system efficiency versus misalignment: 8×2 configuration with SP topology.

4. Parametric Studies

Following the validation of the coupler inductances and the evaluation of the system efficiency with SP compensation, parametric studies have been carried out to analyze the influence of different parameters on the WPT performance. A parametric study allows for the systematic modification and analysis of multiple variables, aiming to enhance the system's overall performance.

To explore alternatives to the challenges identified in the previous configuration, compensation topology and the coils' number of turns were studied, aiming for a coupler configuration with potential improvements. Additionally, a frequency study was carried out to determine the appropriate frequency for the final coupler configuration.

For easy reading, the configurations will be described by $N_1 \times N_2$, where they are composed with N_1 turns for the primary coil and N_2 turns for the secondary coil.

4.1. Compensation Topology and Number of Turns

As an alternative to SP compensation topology, SS topology (Figure 13a) was studied. In this configuration, capacitor C_1 no longer depends on the mutual inductance (Equation (7)), which varies with misalignment.

$$C_1 = \frac{1}{\omega^2 L_1} \quad \& \quad C_2 = \frac{1}{\omega^2 L_2} \quad (7)$$

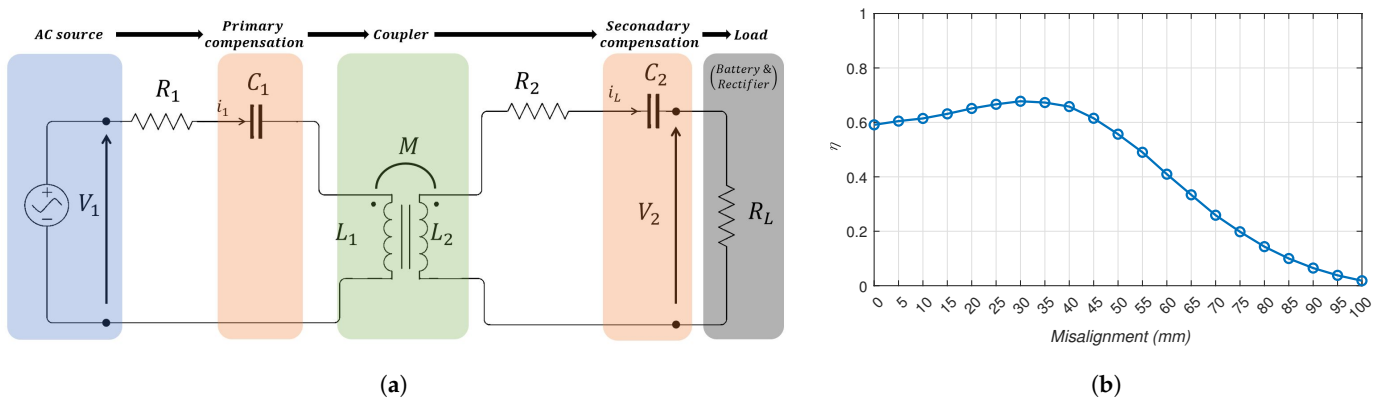


Figure 13. (a) WPT electrical circuit with SS compensation. (b) WPT system efficiency versus misalignment: 8×2 configuration with SS topology.

However, Figure 13b shows lower misalignment tolerance for the 8×2 configuration when SS compensation is adopted. According to [25], to reach high efficiency levels and better misalignment tolerance for this compensation topology for the same frequency, it is preferable to choose a sufficiently high number of turns for both coils.

In order to find an effective and suitable configuration for the number of turns for this compensation topology, different configurations were studied (Table 5).

Table 5. Different configurations tested with SS compensation.

Parameter	4×4	5×5	6×6	8×8
L_1 (μH) at $d_x = 0$ mm	6.94	10.13	13.79	21.8
L_2 (μH) at $d_x = 0$ mm	4.053	6.04	7.87	11.48
M (μH) at $d_x = 0$ mm	1.064	1.415	1.81	3.035
R_{L_1} (m Ω)	81	117	130	246
R_{L_2} (m Ω)	31	39	49	68
C_1 (nF)	158	108	80	51
C_2 (nF)	285	197	148	98
R_{C_1} (m Ω)	50	50	50	50
R_{C_2} (m Ω)	50	50	50	50

Inductances of each configuration were obtained via FEM modeling and measured versus misalignment following the same process previously seen in Sections 3.3 and 3.4. Then, their coupler efficiencies η_{max} were examined (Figure 14).

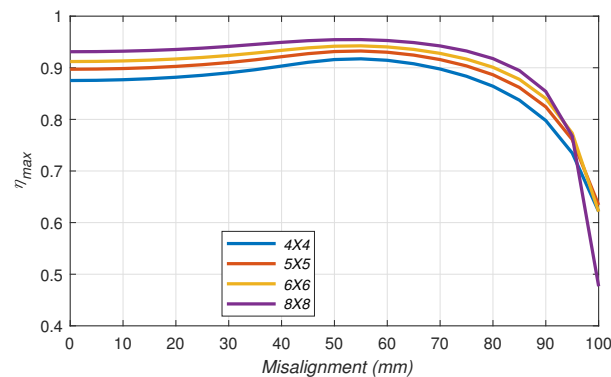


Figure 14. Maximum coupler efficiency of different coupler configurations versus misalignment.

Figure 14 shows efficiency levels of around 90% versus misalignment, up to 80 mm misalignment for all four configurations, with a slight increase of efficiency level with the

number of turns. From 80 mm misalignment onwards, efficiency drops as the receiver coil is mostly outside the perimeter of the transmitter coil, causing weak coupling between coils.

Afterwards, an evaluation of power efficiency was carried out via simulations (Figure 15) to assess the performance of each configuration in real operating conditions.

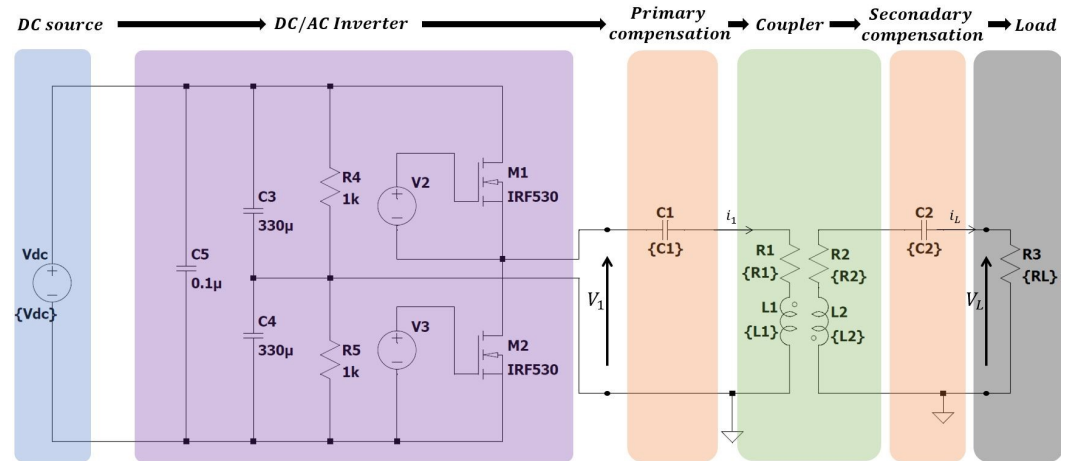


Figure 15. LTspice model of the electrical circuit: SS compensation.

It is important to note that the series resistance of the compensation capacitors was fixed at 50 mΩ (Table 5) to perform the correct comparison between the different configurations studied. These resistances can change depending on how the value of the capacitor was obtained (by taking one capacitor or multiple capacitors in series/in parallel for example) and on the capacitor’s type, and according to these resistances, the efficiency of the WPT system can change, since they are directly related to Joule losses in the system.

Results of the simulations (Figure 16) show that the more turns the coils contain, the better the efficiency and the tolerance to misalignment; configurations 6 × 6 and 8 × 8 have close efficiencies of approximately 78% with misalignment tolerances up to 75 mm.

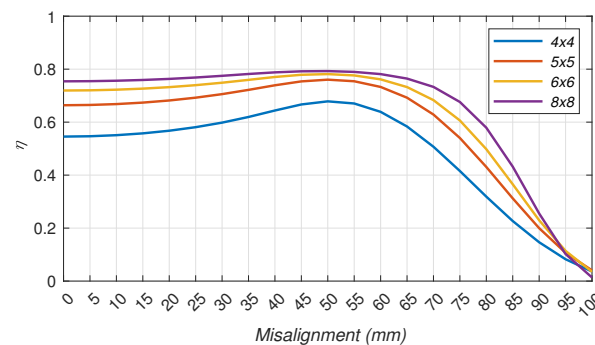


Figure 16. WPT system efficiency versus misalignment of different configurations: SS compensation.

The difference in tolerance to misalignment between the maximum coupler efficiency curves (Figure 14) that can go up to 90 mm misalignment and power efficiency curves (Figure 16) that can undergo 75 mm misalignment is that in power efficiency evaluation, compensation capacitors are taken into account, and beyond 75 mm misalignment, capacitor C₁ no longer provides full compensation. At this misalignment distance, the primary inductance changes due to the proximity of the two coils and the displacement of the ferrite above the secondary coil, affecting the overall system performance.

The choice between the 6 × 6 and 8 × 8 configurations favors the configuration 6 × 6. This configuration has fewer turns on the receiving part compared to the configuration 8 × 8, which is crucial for reducing the weight of the secondary block to be integrated into the UAV. Furthermore, according to Figure 17, this configuration presents more tolerance

to misalignment than the 8×2 configuration with SP compensation presented in Figure 12, which is why this configuration, with SS compensation, will be tested in Section 5 for experimental validation.

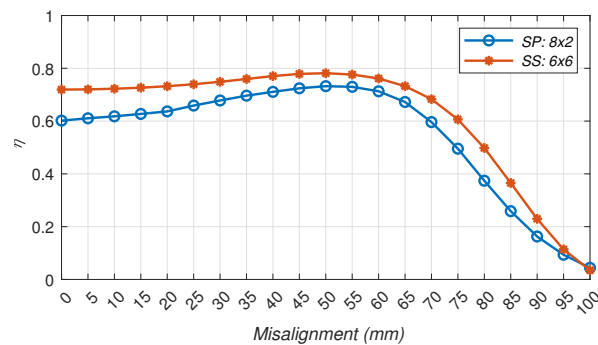


Figure 17. Simulated efficiency of SS compensation and SP compensation versus misalignment.

In other cases, where the misalignment tolerance is a higher priority than weight, configuration 8×8 might be a better choice. Therefore, the results of these studies will depend on the specific objectives sought.

4.2. Frequency Study

In order to check the frequency choice, the maximum coupler efficiency (Equation (1)) of the 6×6 configuration with SS compensation was analyzed at perfect alignment across different frequencies.

Figure 18 shows the coupler efficiency augmentation with frequency increase. For a 80 to 90% coupler efficiency, the frequency must be at least 115 kHz. Opting for 150 kHz ensures a satisfying choice for efficiency. Choosing higher frequency can lead to higher switching losses and higher electromagnetic interference.

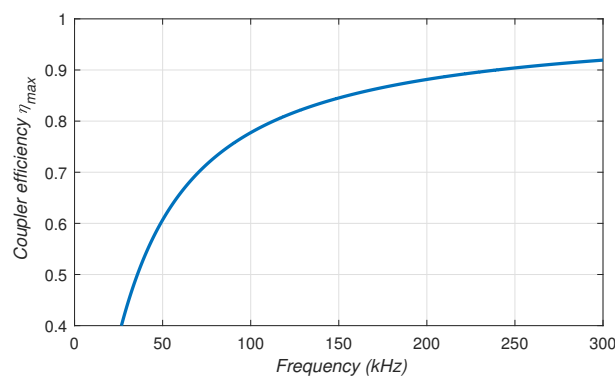


Figure 18. Coupler efficiency versus frequency: SS compensation.

Once the frequency and coupler configuration were determined, experimental testing of the system was carried out in order to validate simulation results and system performance.

5. Experimental Test Bench

The test bench used to measure the power efficiency of the WPT system and to validate the simulation model is shown in Figures 19 and 20. The setup consists of a DC power source, an inverter, a primary compensation capacitor connected to the coupler, a secondary compensation capacitor and an equivalent resistive load. An oscilloscope is used to visualize the currents and voltages present in the system. The receiver coil is mounted on a controlled mechanic arm to enable misalignment studies.

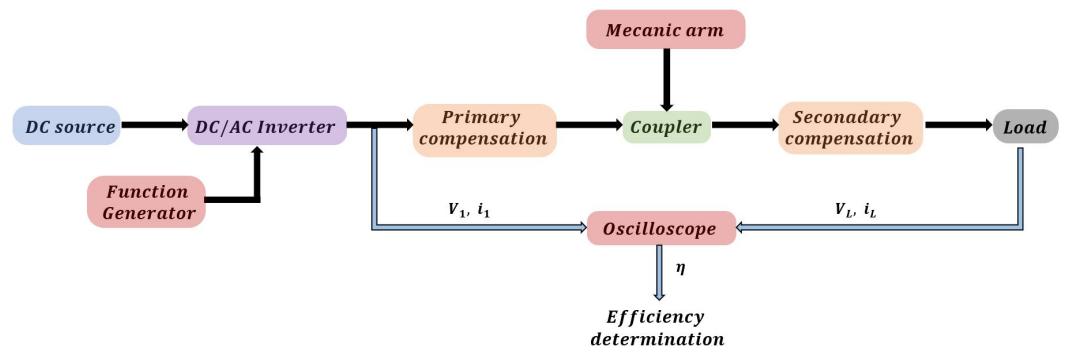


Figure 19. Connections of the Experimental Setup.

A reduced-power model of the WPT system was implemented, multiple tests were run under misalignment conditions, and the system’s efficiency was evaluated versus misalignment. The settings of the experimental bench are described in Table 6.

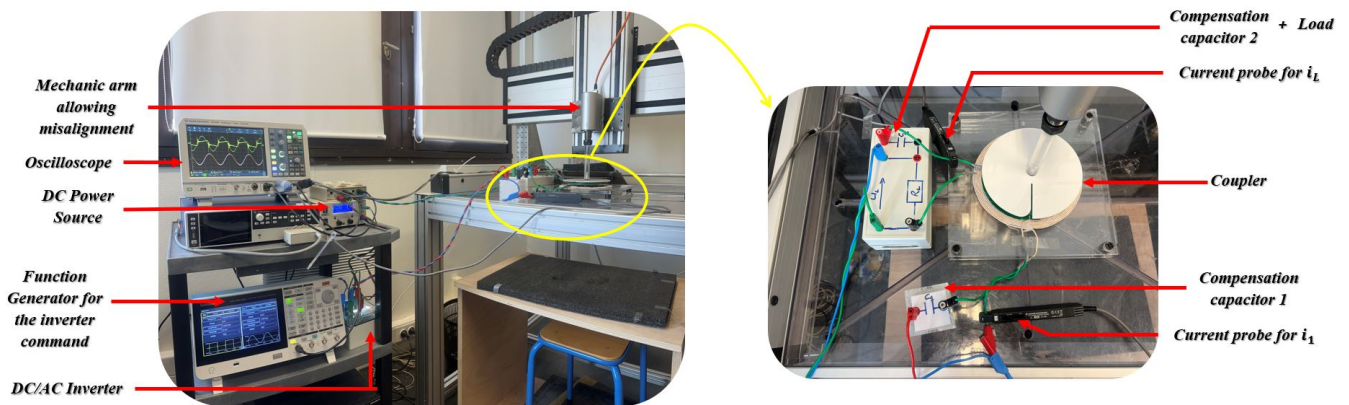


Figure 20. Experimental test bench.

Table 6. Experimental bench specifications.

Parameter	Symbol	Value	Unit
Source power (AC)	P_1	up to 77	W
Load power	P_L	up to 48.2	W
T_x self-inductance at $d_x = 0$ mm	L_1	13.8	μH
R_x self-inductance at $d_x = 0$ mm	L_2	7.9	μH
Mutual inductance at $d_x = 0$ mm	M	1.81	μH
Primary bloc resistance ($R_{L_1} + R_{C_1} + \text{cables}$)	R_1	180	$\text{m}\Omega$
Secondary bloc resistance ($R_{L_2} + R_{C_2} + \text{cables}$)	R_2	112	$\text{m}\Omega$
Load equivalent resistance	R_L	2	Ω
Primary capacitor	C_1	78	nF
Secondary capacitor	C_2	158	nF

Figure 21 shows the time response of the source and load voltages and currents for two misalignment cases: 0 mm and 90 mm. In the first case of 0 mm misalignment, the obtained curves show correlation with the simulation results (Figure 11) with a difference in power level. This correspondence indicates that the model accurately simulates the essential characteristics of the real system, such as resonances and losses.

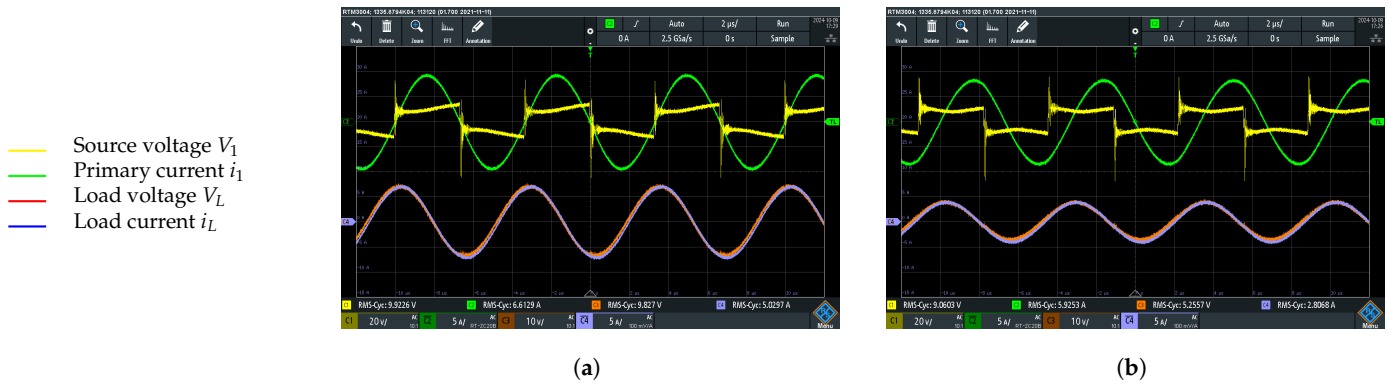


Figure 21. Experimental voltage and current of source and load. (a) $d_x = 0$ mm. (b) $d_x = 90$ mm.

At 90 mm misalignment, a phase shift between the primary current and voltage is observed. This is due to weak coupling and variation in the transmitter self inductance L_1 caused by the proximity of the ferrite on top of the secondary coil, which led to losing the compensation on the primary bloc.

Results Analysis

The RMS values of the currents and voltages were measured for each case of misalignment to calculate the power efficiency of the system (Equation (4)) versus misalignment.

The efficiency curves from both experimental and simulation results (Figure 22) exhibit similar trends with an error margin of less than 10%. The efficiency level remains between 70 and 80%. This is largely due to the chosen operating frequency (Figure 18), where the maximum achievable efficiency of the coupler was observed to be approximately 85–90% at 150 kHz. Additionally, Joule losses in the components further reduce the overall system efficiency to 70–80% with a misalignment tolerance limit of 75 mm. Beyond this point, the system operates at an efficiency below 70%.

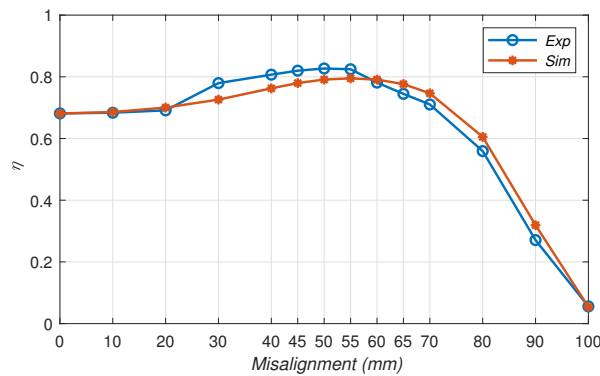


Figure 22. WPT system efficiency versus misalignment.

It is possible to improve the system’s efficiency level by increasing frequency; however, higher frequencies can lead to higher switching losses and higher electromagnetic interference to explore.

6. Conclusions

The parametric approach presented in this paper identified a 6×6 configuration with SS compensation topology as the recommended configuration for the DJI F450 UAV. The analysis of key parameters «compensation topology, number of turns of coils and frequency» effectively enhanced the performance of the WPT system. Compensation topology and number of turns of coils were found to have an impact on the system’s tolerance to misalignment. Experimental tests confirmed the accuracy of the FEM and simulation models for an improved coupler design approach. In addition, the frequency

choice showed a significant impact on the overall system performance. These results highlight the importance of a comprehensive parametric analysis to improve the efficiency and performance of the WPT system and pave the way for further perspectives using algorithmic optimization. Another very important aspect to be taken into account in future explorations is the study of the electromagnetic compatibility (EMC) of the designed system, which should be safe enough for the UAV's on-board electronics.

Author Contributions: Methodology and validation, M.T., M.-K.S. and M.B.; software, M.T.; writing—original draft preparation, M.T.; writing—review and editing, M.-K.S., M.B. and L.P.; Supervision, L.P. All authors have read and agreed to the published version of the manuscript.

Funding: This research received no external funding.

Data Availability Statement: The datasets presented in this article are not readily available because the data are part of an ongoing study. Requests to access the datasets should be directed to M.-K.S.

Conflicts of Interest: The authors declare no conflicts of interest.

References

- Jawad, A.; Jawad, H.; Nordin, R.; Gharghan, S.; Abdullah, N.; Abu Al-Shaeer, M. Wireless Power Transfer with Magnetic Resonator Coupling and Sleep/Active Strategy for a Drone Charging Station in Smart Agriculture. *IEEE Access* **2019**, *7*, 139839–139851. [[CrossRef](#)]
- Skorput, P.; Mandzuka, S.; Vojvodić, H. The use of Unmanned Aerial Vehicles for forest fire monitoring. In Proceedings of the 2016 International Symposium ELMAR, Zadar, Croatia, 12–14 September 2016; pp. 93–96. [[CrossRef](#)]
- Ke, D.; Chunhua, L.; Jiang, C.; Zhao, F. Design of an effective wireless air charging system for electric unmanned aerial vehicles. In Proceedings of the IECON 2017—43rd Annual Conference of the IEEE Industrial Electronics Society, Beijing, China, 29 October 2017–1 November 2017; pp. 6949–6954. [[CrossRef](#)]
- Duan, S.; Lu, X.; Wu, H.; Zhang, H.; Zhang, Z.; Wang, G. Unmanned Aerial Vehicle Wireless Power Transfer System for Long-Distance Transmission Line Patrol. In Proceedings of the IEEE International Power Electronics and Application Conference and Exposition (PEAC), Guangzhou, China, 4–7 November 2022; pp. 1324–1329. [[CrossRef](#)]
- Moraes, L.; Carmo, L.; Campos, R.; da Silva Junior, M.A.; Moreira, L.; Carvalho de Souza, J.; Teixeira, A.; Silveira, D.; Coelho, T.; Luis, A.; et al. Autonomous Quadrotor for accurate positioning. *IEEE Aerosp. Electron. Syst. Mag.* **2017**, *32*, 58–62. [[CrossRef](#)]
- Kang, S.H.; Choi, J.H.; Harackiewicz, F.; Jung, C.W. Magnetic Resonant Three-Coil WPT System Between Off/In-Body for Remote Energy Harvest. *IEEE Microw. Wirel. Components Lett.* **2016**, *26*, 741–743. [[CrossRef](#)]
- Gao, X.; Liu, C.; Huang, Y.; Song, Z. Design of An UAV-Oriented Wireless Power Transfer System with Energy-Efficient Receiver. In Proceedings of the IECON 2020 the 46th Annual Conference of the IEEE Industrial Electronics Society, Singapore, 18–21 October 2020; pp. 2025–2030. [[CrossRef](#)]
- Duan, S.; Zhang, H.; Wang, Y.; Zhen, W.; Zhang, Z.; Yu, T. Unmanned Aerial Vehicle Wireless Power Transfer System with Light-Weight and Low Leakage Flux Interference. In Proceedings of the 2022 IEEE International Power Electronics and Application Conference and Exposition (PEAC), Guangzhou, China, 4–7 November 2022; pp. 1481–1485. [[CrossRef](#)]
- Song, C.; Kim, H.; Jung, D.H.; Yoon, K.; Cho, Y.; Kong, S.; Kwack, Y.; Kim, J. Three-Phase Magnetic Field Design for Low EMI and EMF Automated Resonant Wireless Power Transfer Charger for UAV. In Proceedings of the 2015 IEEE Wireless Power Transfer Conference (WPTC), Boulder, CO, USA, 13–15 May 2015; pp. 1–4. [[CrossRef](#)]
- Li, X.; Lu, J.; Stegen, S. Magnetic Coupler Optimization for Inductive Power Transfer System of Unmanned Aerial Vehicles. *Energies* **2021**, *14*, 7024. [[CrossRef](#)]
- Campi, T.; Cruciani, S.; Maradei, F.; Feliziani, M. Innovative Design of Drone Landing Gear Used as a Receiving Coil in Wireless Charging Application. *Energies* **2019**, *12*, 3483. [[CrossRef](#)]
- Campi, T.; Dionisi, F.; Cruciani, S.; De Santis, V.; Feliziani, M.; Maradei, F. Magnetic field levels in drones equipped with Wireless Power Transfer technology. In Proceedings of the 2016 Asia-Pacific International Symposium on Electromagnetic Compatibility (APEMC), Shenzhen, China, 17–21 May 2016; pp. 544–547. [[CrossRef](#)]
- Eid, A.; Rich, N.; Hattori, A.; Chen, I.-T.; Hester, J.; Tentzeris, M.M. Deployable Origami Coils for Wireless UAV in-Flight Powering. In Proceedings of the 2023 IEEE Wireless Power Technology Conference and Expo (WPTCE), San Diego, CA, USA, 4–8 June 2023; pp. 1–4. [[CrossRef](#)]
- Sang-Won, K.; In-Kui, C.; Sung-Yong, H. Comparison of charging region differences according to receiver structure in drone wireless charging system. In Proceedings of the 2017 International Conference on Information and Communication Technology Convergence (ICTC), Jeju, Republic of Korea, 18–20 October 2017; pp. 1058–1060. [[CrossRef](#)]
- Nguyen, B.X.; Vilathgamuwa, D.; Foo, G.; Wang, P.; Ong, A.; Madawala, U.; Nguyen, T.D. An Efficiency Optimization Scheme for Bidirectional Inductive Power Transfer Systems. *IEEE Trans. Power Electron.* **2015**, *30*, 6310–6319. [[CrossRef](#)]
- Kadem, K.; Bensetti, M.; Le Bihan, Y.; Labouré, E.; Debbou, M. Optimal Coupler Topology for Dynamic Wireless Power Transfer for Electric Vehicle. *Energies* **2021**, *14*, 3983. [[CrossRef](#)]

17. Vedavyas Manjunath, D.; Lakshmi Priya, G.; Vaishnavi, R.; Bobba, P.B. Analysis of Different Coil Structures used in Wireless Power Transfer based UAVs. In Proceedings of the 2022 IEEE 2nd International Conference on Sustainable Energy and Future Electric Transportation (SeFeT), Hyderabad, India, 4–6 August 2022; pp. 1–6. [[CrossRef](#)]
18. Pham, T.S.; Nguyen, T.D.; Tung, B.S.; Khuyen, B.X.; Hoang, T.T.; Ngo, Q.M.; Hiep, L.T.H. Optimal frequency for magnetic resonant wireless power transfer in conducting medium. *Sci. Rep.* **2021**, *11*, 18690. [[CrossRef](#)] [[PubMed](#)]
19. Bosshard, R.; Mühlethaler, J.; Kolar, J.W.; Stevanović, I. Optimized magnetic design for inductive power transfer coils. In Proceedings of the 2013 Twenty-Eighth Annual IEEE Applied Power Electronics Conference and Exposition (APEC), Long Beach, CA, USA, 17–21 March 2013; pp. 1812–1819. [[CrossRef](#)]
20. Turki, F.; Wiengarten, R.; Reising, V.; Kratser, A. Impact of the Working Frequency on Wireless Power Transfer Systems. In Proceedings of the PCIM Europe 2014; International Exhibition and Conference for Power Electronics, Intelligent Motion, Renewable Energy and Energy Management, Nuremberg, Germany, 20–22 May 2014; pp. 1–6.
21. Pang, S.; Xu, J.; Xie, Z.; Lu, J.; Li, H.; Li, X. Lightweight UAV's Wireless Power Transfer System for Constant Current Charging Without Secondary Feedback Control. *IEEE Trans. Veh. Technol.* **2023**, *72*, 15611–15621. [[CrossRef](#)]
22. Lu, M.; Ngo, K.D.T. Analytical Calculation of Proximity-Effect Resistance for Planar Coil with Litz Wire and Ferrite Plate in Inductive Power Transfer. *IEEE Trans. Ind. Appl.* **2019**, *55*, 2984–2991. [[CrossRef](#)]
23. Trivino-Cabrera, A. Compensation Networks. In *Wireless Power Transfer for Electric Vehicles: Foundations and Design Approach*; Springer: Berlin/Heidelberg, Germany, 2019; pp. 69–98.
24. Campi, T.; Cruciani, S.; Feliziani, M. Wireless Power Transfer Technology Applied to an Autonomous Electric UAV with a Small Secondary Coil. *Energies* **2018**, *11*, 352. [[CrossRef](#)]
25. Enssle, A.; Parspour, N. Power Loss Shifted Design of Inductive Energy Transfer Systems. *EEE Open J. Power Electron.* **2020**, *1*, 113–123. [[CrossRef](#)]

Disclaimer/Publisher's Note: The statements, opinions and data contained in all publications are solely those of the individual author(s) and contributor(s) and not of MDPI and/or the editor(s). MDPI and/or the editor(s) disclaim responsibility for any injury to people or property resulting from any ideas, methods, instructions or products referred to in the content.